Biochimica et Biophysica Acta 1838 (2014) 2807–2816

Contents lists available at ScienceDirect

Biochimica et Biophysica Acta

journal homepage: www.elsevier.com/locate/bbamem

Temperature-sensitive paramagnetic liposomes for image-guided drug delivery: Mn^{2+} versus [Gd(HPDO3A)(H_2O)]

Sin Yuin Yeo [a,c], Mariska de Smet [a,c], Sander Langereis [b,c], Luce Vander Elst [d], Robert N. Muller [d,e], Holger Grüll [a,b,c,*]

[a] Department of Biomedical Engineering, Biomedical NMR, Eindhoven University of Technology, Eindhoven, The Netherlands
[b] Department of Minimally Invasive Healthcare, Philips Research Eindhoven, Eindhoven, The Netherlands
[c] Center for Imaging Research and Education (CIRE), Eindhoven, The Netherlands
[d] Department of General, Organic and Biomedical Chemistry, NMR and Molecular Imaging Laboratoy, University of Mons, Belgium
[e] Center for Microscopy and Molecular Imaging, Charleroi, Belgium

ARTICLE INFO

Article history:
Received 12 April 2014
Received in revised form 29 June 2014
Accepted 15 July 2014
Available online 28 July 2014

Keywords:
Temperature-sensitive liposomes
Manganese
[Gd(HPDO3A)(H2O)]
Image-guided drug delivery
Hyperthemia
Doxorubicin

ABSTRACT

Temperature-sensitive liposomes (TSLs) loaded with doxorubicin (Dox), and Magnetic Resonance Imaging contrast agents (CAs), either manganese (Mn^{2+}) or [Gd(HPDO3A)(H_2O)], provide the advantage of drug delivery under MR image guidance. Encapsulated MRI CAs have low longitudinal relaxivity (r_1) due to limited transmembrane water exchange. Upon triggered release at hyperthermic temperature, the r_1 will increase and hence, provides a means to monitor drug distribution in situ. Here, the effects of encapsulated CAs on the phospholipid bilayer and the resulting change in r_1 were investigated using MR titration studies and ^{1}H Nuclear Magnetic Relaxation Dispersion (NMRD) profiles. Our results show that Mn^{2+} interacted with the phospholipid bilayer of TSLs and consequently, reduced doxorubicin retention capability at 37 °C within the interior of the liposomes over time. Despite that, Mn^{2+}-phospholipid interaction resulted in higher r_1 increase, from 5.1 ± 1.3 mM^{-1} s^{-1} before heating to 32.2 ± 3 mM^{-1} s^{-1} after heating at 60 MHz and 37 °C as compared to TSL(Gd,Dox) where the longitudinal relaxivities before and after heating were 1.2 ± 0.3 mM^{-1} s^{-1} and 4.4 ± 0.3 mM^{-1} s^{-1}, respectively. Upon heating, Dox was released from TSL(Mn,Dox) and complexation of Mn^{2+} to Dox resulted in a similar Mn^{2+} release profile. From 25 to 38 °C, r_1 of [Gd(HPDO3A)(H_2O)] gradually increased due to increase transmembrane water exchange, while no Dox release was observed. From 38 °C, the release of [Gd(HPDO3A)(H_2O)] and Dox was irreversible and the release profiles coincided. By understanding the non-covalent interactions between the MRI CAs and phospholipid bilayer, the properties of the paramagnetic TSLs can be tailored for MR guided drug delivery.

1. Introduction

In 1978, Yatvin et al. proposed the concept of temperature-triggered release of a chemotherapeutic drug from the aqueous lumen of temperature-sensitive liposomes (TSLs) composed of 1,2-dipalmitoyl-*sn*-glycerol-3-phosphatidylcholine (DPPC) and 1,2-distearoyl-*sn*-glycerol-3-phospatidylcholine (DSPC). The drug remains encapsulated in the inner compartment of the TSLs at body temperature, whereas the drug is released at temperatures close to the melting phase transition temperature (T_m) of the lipid bilayer [1]. For application in hyperthermia-mediated drug delivery, TSLs are injected intravenously and release their payload in tumor tissues that are externally heated to 41–42 °C. With this local drug delivery approach, high concentration of drugs is reached at the tumor site, thereby expanding the therapeutic window [2–4]. A milestone in the development of TSLs was the incorporation of lyso-phospholipids in the lipid bilayer, which speeds up the drug release kinetic and facilitates quantitative drug release [5,6]. The development of TSLs and their applications are comprehensively reviewed by Landon et al. [7].

The concept of temperature-triggered drug release under magnetic resonance (MR)-image guidance has been exploited by Viglianti et al. [8–11] and de Smet et al. [2,12–14] using manganese (Mn^{2+}) and [Gd(HPDO3A)(H_2O)] loaded liposomal doxorubicin (Dox), respectively. This approach embarks on earlier research of using paramagnetic liposomes loaded with Mn^{2+} [15,16] or Gd-chelates [2,17–25] as magnetic resonance imaging (MRI) contrast agents (CAs). Encapsulation of paramagnetic compounds in the lumen of a liposome leads to an apparent reduction of the ionic longitudinal relaxivity (r_1) as the water exchange between the lumen and the surroundings is hampered by slow water

* Corresponding author at: Department of Biomedical Engineering, Eindhoven University of Technology, Den Dolech 2, 5600 MB Eindhoven, The Netherlands. Tel.: +31 612932309.
E-mail address: h.gruell@tue.nl (H. Grüll).

http://dx.doi.org/10.1016/j.bbamem.2014.07.019
0005-2736/

diffusion across the lipid bilayer. Subsequent release of the paramagnetic CAs from the liposomal carriers then restores the r_1, which has been exploited to quantify [26,27] and image this process with MRI [21]. However, the situation is more complicated for Mn^{2+} as it has been demonstrated that Mn^{2+} interacts with the negatively charged phospholipid head groups leading to an increase of its r_1 as the rotational correlation time increases [15]. As Mn^{2+} complexes Dox via the anthraquinone (hydroxyketone) moieties and the amino-sugar group, it can also be used as a liposomal loading agent [28–30]. For image-guided drug delivery, the interaction of Mn^{2+} and Dox has the advantage of ensuring concurrent release of both compounds from the interior of the TSLs. Upon release from the interior of the liposomes, Mn^{2+} interacts with the negatively charged phospholipid bilayer in the surrounding tissue which prolongs or even prohibits the wash out from the tumor tissue to allow for better correlation with drug distribution. Viglianti et al. demonstrated that the change in the longitudinal relaxation rate (ΔR_1), a consequence of co-release of Mn^{2+} and Dox, can be exploited to monitor, localize and quantify drug release in vivo [10]. Although preclinical results show promising application of TSLs containing Mn^{2+} and Dox for drug delivery and dose painting [8,10], further development of such TSLs is hindered potentially by the cellular toxicity of Mn^{2+} [31–33]. Alternatively, [Gd(HPDO3A)(H_2O)], a clinically approved MRI CA has been co-encapsulated with Dox in the TSLs [2,13,18]. Similar to Mn^{2+}, release of [Gd(HPDO3A)(H_2O)] from the TSLs at elevated temperatures enhances the MR signal in the surrounding tissue. However, [Gd(HPDO3A)(H_2O)] is an extravascular, extracellular CA that is rapidly cleared from the circulation via renal excretion [34]. For application in highly vascularized tumors, the rapid wash out of [Gd(HPDO3A)(H_2O)] may complicate the quantification of drug concentration in situ as the pharmacokinetic and free volume of distribution of [Gd(HPDO3A)(H_2O)] and Dox are different.

Given the advantages and disadvantages of co-encapsulating Mn^{2+} and [Gd(HPDO3A)(H_2O)] with a chemotherapeutic drug, the choice of paramagnetic TSLs for in vivo use should be made wisely and tailored to a specific application. To date, these two temperature-sensitive paramagnetic liposomal Dox formulations were evaluated using different phospholipid compositions and experimental conditions, making a direct comparison difficult. As one of the main benefits of paramagnetic TSLs is visualization of local drug delivery, in depth understanding of the ΔR_1 due to the type of CA encapsulated is crucial and warranted to ensure accurate quantification of local drug concentration. In this paper, the interaction of the encapsulated Mn^{2+} and [Gd(HPDO3A)(H_2O)] with the phospholipid bilayer (Fig. 1), and the change in r_1 associated with this interaction, as well as effects on stability of the formulation are investigated in great detail through a series of MR titration studies and ^1H nuclear magnetic relaxation dispersion (NMRD) profiles.

2. Materials and methods

2.1. Materials

1,2-Dipalmitoyl-*sn*-glycerol-3-phosphatidylcholine (DPPC), 1-palmitoyl-2-hydroxy-*sn*-glycero-3-phosphocholine (MPPC) and 1,2-dipalmitoyl-*sn*-glycero-3-phosphoethanolamine-N-[methoxy(polyethylene glycol)2000] (DPPE-PEG_{2000}), were purchased from Avanti Polar Lipids, Inc. [Gd(HPDO3A)(H_2O)] (ProHance®) was obtained from Bracco Diagnostics. Dox was purchased from AvaChem Scientific and manganese sulfate ($MnSO_4$) was purchased from Sigma-Aldrich.

2.2. Liposome preparation

All TSLs were prepared by using a lipid film hydration technique, where DPPC, MPPC and DPPE-PEG_{2000} were combined in a molar ratio of 86:10:4. A total of 115 μmol phospholipid was dissolved in a chloroform:methanol solution of ratio 4:1 (*v*/*v*). The solvent was evaporated using a rotary evaporator at 32 °C and a pressure of 20 mbar for one

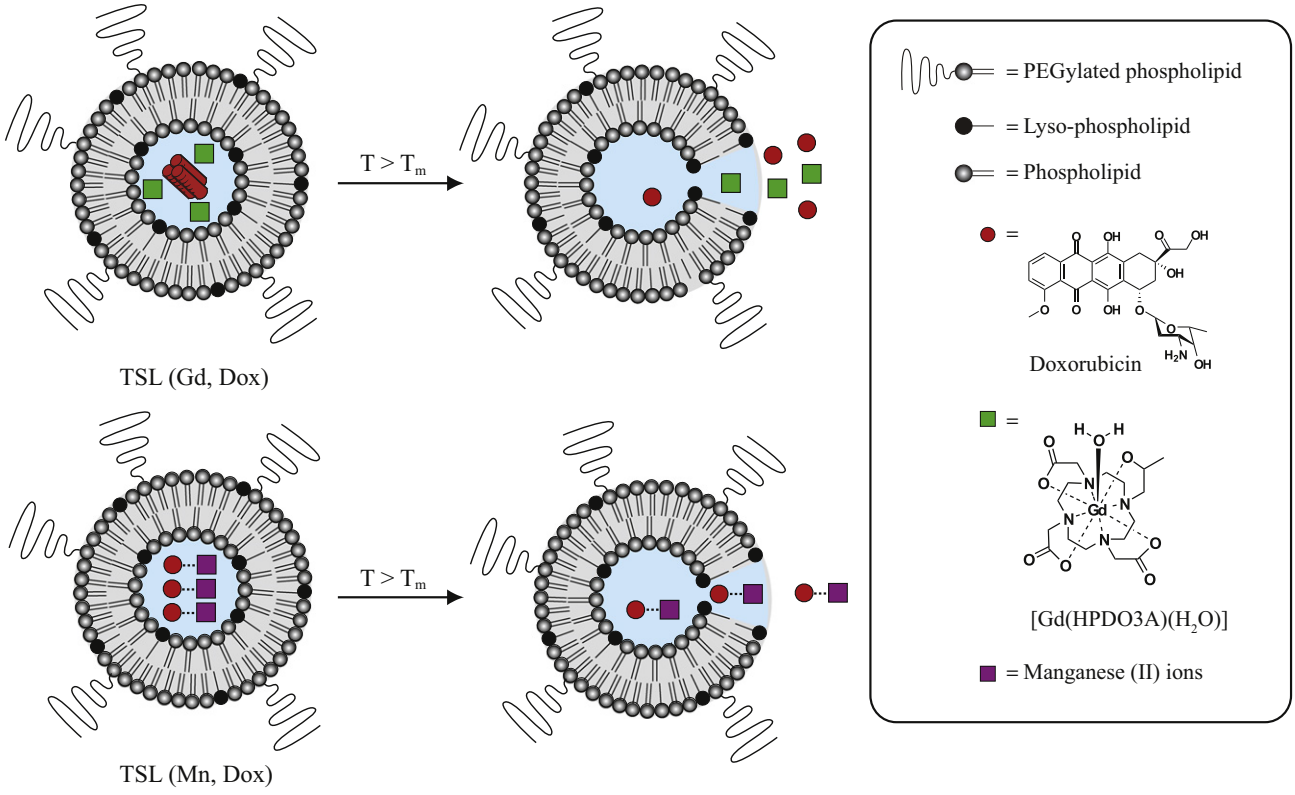

Fig. 1. Schematic representation of temperature-induced delivery of MRI CAs and Dox at the T_m of the lipid bilayer. Dashed lines show the non-covalent interaction of Mn^{2+} and Dox with the negatively charged phospholipid bilayer of the temperature-sensitive liposome.

hour. The resulting lipid films were hydrated at 60 °C with either 4.5 mL of 300 mM ammonium sulfate [$(NH_4)_2SO_4$] (empty TSLs), 4.5 mL of 300 mM $MnSO_4$ [TSL(Mn)] or 4.5 mL of 300 mM [Gd(HPDO3A)(H_2O)] and 120 mM [$(NH_4)_2SO_4$] mixture [TSL(Gd)], all having a pH of 3.5. Large multilamellar vesicles were downsized by successive extrusion through 400 nm filters (two times), 200 nm filters (two times) and 100 nm filters (five times) at 60 °C. Following extrusion, the extraliposomal buffers were replaced by performing dialysis against 300 mM sucrose/20 mM HEPES buffer at pH 7.5. Next, Dox (5 mg/mL 300 mM sucrose/20 mM HEPES) was added to all liposomes at a drug-to-lipid weight ratio 0.05 to 1 and incubated at 33 °C for 90 min. The unencapsulated Dox was removed by fractionating all liposomes through PD-10 columns. TSLs containing Mn^{2+} and Dox [TSL(Mn, Dox)] were royal purple, whereas TSLs containing [Gd(HPDO3A)(H_2O)] and Dox [TSL(Gd,Dox)] were orange. Three batches of liposomes were prepared for each formulation.

2.3. Liposome characterizations

Phospholipid concentrations were determined based on the Rouser method [35]. Intraliposomal Mn^{2+} and [Gd(HPDO3A)(H_2O)] concentrations were determined by using Inductively Coupled Plasma-Mass Spectrometry (ICP-MS, DRCII, Perkin Elmer). For determination of Dox concentration, liposomes were destructed with Triton X-100 and the amount of fluorescence was measured at λ_{ex} of 485 nm and λ_{em} of 590 nm (Perkin Elmer LS55).

Hydrodynamic radii (r_h) of liposomes were determined using Dynamic Light Scattering (DLS) (ALV/CGS-3 Compact Goniometer System, ALV-GmbH, Langen, Germany). The hydrodynamic r_h was calculated from the diffusion coefficient $r_h = kT/(6\pi\eta D)$ and corrected for the viscosity of the sucrose containing buffer, $\eta = 1.33$ Pa·s.

Differential Scanning Calorimetry (DSC) (Q2000 DSC, TA Instruments, USA) was used to determine the T_m of the lipid bilayer. T_m is described as the temperature at the onset of the DSC thermogram. All samples were heated from 20 to 70 °C at 5 K/min.

The morphologies of TSLs were studied using cryogenic transmission electron microscopy (cryo-TEM). Samples were prepared using a Vitrobot and studied using a FEI TECNAI F30ST at 300 kV. Subsequently, images were recorded using a CCD camera (1 k × 1 k) [13].

2.4. MR titration studies/binding studies

Titration experiments were performed by addition of empty TSLs to $MnSO_4$ (0.3 mM) and [Gd(HPDO3A)(H_2O)] (0.3 mM) solutions to assess the effects of potential phospholipid and CA interactions on r_1. The longitudinal relaxation times (T_1) of $MnSO_4$ and [Gd(HPDO3A)(H_2O)] solutions prior to addition of TSLs (22 mM phospholipid) were measured using Minispec 60 (Bruker, Ettlingen, Germany) at 37 °C. Next, 10 μL of TSLs was added to 190 μL of each sample and T_1 was measured as well. The experiment involved addition of ten times 10 μL of empty TSLs (22 mM phospholipid) and T_1 was recorded after each addition. From these measurements, r_1 was calculated based on Eq. (1).

$$r_1 = \left[\left({}^1\!/_{T1}\right) - \left({}^1\!/_{T1,0}\right)\right] / [CA] \quad (1)$$

where $T_{1,0}$ is the T_1 of sucrose buffer, T_1 represents the measured T_1 before or after heating and [CA] is the concentration of CAs in mM and corrected for the dilution due to addition of TSLs. The r_1 was plotted against the phospholipid-to-CA concentration ratio.

The titration data were fitted with a mathematical model, which describes the non-covalent binding of CA to the phospholipid bilayer of TSLs (P) with N identical, independent binding sites [36,37]. From this model, the binding stoichiometry between CA and phospholipids (N), r_1 of CA bound to phospholipids ($r_{1,\,bound}$), and the association constant (K_a) were determined based on Eq. (2).

$$r_1 = r_{1,\text{bound}} + (r_{1,\text{free}} - r_{1,\text{bound}}) \times \left[{}^1\!/_2 + \frac{1}{2K_a[CA]} - N \times \frac{[P]}{2[CA]} + \sqrt{\left(\frac{1}{2K_a[CA]} - {}^1\!/_2 + N \times \frac{[P]}{2[CA]}\right)^2 + \frac{1}{K_a[CA]}}\right] \quad (2)$$

where r_1 is determined experimentally ($mM^{-1}\,s^{-1}$), $r_{1,free}$ is the relaxivity of free CA ($mM^{-1}\,s^{-1}$), $r_{1,bound}$ is the longitudinal relaxivity of CA bound to phospholipids ($mM^{-1}\,s^{-1}$), K_a is the association constant (M^{-1}), [P] is the phospholipid concentration (M) and [CA] is the CA concentration (M). For fitting, the longitudinal relaxivity of Mn^{2+} was set to $r_{1,free} = 6.9\ mM^{-1}\,s^{-1}$.

2.5. Interaction of CAs with phospholipid bilayer after release

TSL(Mn) was prepared at a Mn^{2+} concentration of 0.25 mM. T_1 was measured using Minispec 60 at 37 °C. Subsequently, the sample was heated to 42 °C for 15 min to ensure complete release of encapsulated Mn^{2+}, cooled to 37 °C and T_1 was measured (Fig. 2). In a second set of experiments, TSL(Mn) containing 0.25 mM Mn^{2+} was heated to 42 °C for 15 min and cooled to 37 °C. The released Mn^{2+} was physically separated from TSLs using a 50 kDa Vivaspin ultrafiltration spin column. The pellets remaining at the filters were resuspended in 200 μL sucrose buffer. T_1 of the supernatant (released intraliposomal contents) and pellets (TSLs) were measured at 37 °C (Fig. 2). Similar procedures were performed for TSL(Mn,Dox) ([Mn^{2+}] = 0.29 mM), TSL(Gd) ([Gd(HPDO3A)(H_2O)] = 1.52 mM) and TSL(Gd,Dox) ([Gd(HPDO3A)(H_2O)] = 1.59 mM). Two independent measurements were performed for all samples, final concentration of Mn^{2+} and Gd^{3+} in each sample was measured using ICP-MS and r_1 were calculated using Eq. (1).

2.6. ^{1}H nuclear magnetic relaxation dispersion (NMRD)

^{1}H NMRD of 500 μL TSL(Mn,Dox) was measured at 35 °C to prevent premature release of CAs from interior of the liposomes. Subsequently, the sample was heated to 42 °C for 20 min, cooled down to 35 °C in a water bath, and ^{1}H NMRD was measured again at 35 °C. A second sample was prepared by adding a mixture of Mn^{2+} and Dox (Mn + Dox) to empty TSLs, and subjected to a similar ^{1}H NMRD measurement (TSL + Mn + Dox). The TSL + Mn + Dox measurements were required to compare the effects of externally added Mn + Dox to intraliposomally released Mn + Dox on r_1 at different magnetic fields. As a control, a ^{1}H NMRD of Mn + Dox with a similar Mn^{2+}-to-Dox concentration ratio and Mn^{2+} were measured at 35 °C.

Similarly, ^{1}H NMRD of [Gd(HPDO3A)(H_2O)] in 500 μL of TSL(Gd, Dox) was measured at 35 °C before and after heat treatment. A separate sample was prepared by adding a mixture of [Gd(HPDO3A)(H_2O)] and Dox (Gd + Dox) to TSLs, and subjected to the same ^{1}H NMRD measurement (TSL + Gd + Dox). As a control, ^{1}H NMRD of Gd + Dox with a similar [Gd(HPDO3A)(H_2O)]-to-Dox concentration ratio and [Gd(HPDO3A)(H_2O)] was determined at 35 °C.

Samples were prepared in a 300 mM sucrose/20 mM HEPES buffer at pH 7.5. Table 1 summarizes all measured samples and their respective CA, Dox and phospholipid concentrations.

All ^{1}H NMRD profiles were measured at magnetic field strengths ranging from 0.02 to 40 MHz using a Stelar SpinMaster FFC-2000 relaxometer, 60 MHz using Minispec 60 (Bruker, Ettlingen, Germany) and 300 MHz using a 300 MHz high-resolution NMR spectrometer (Bruker Avance, Ettlingen, Germany).

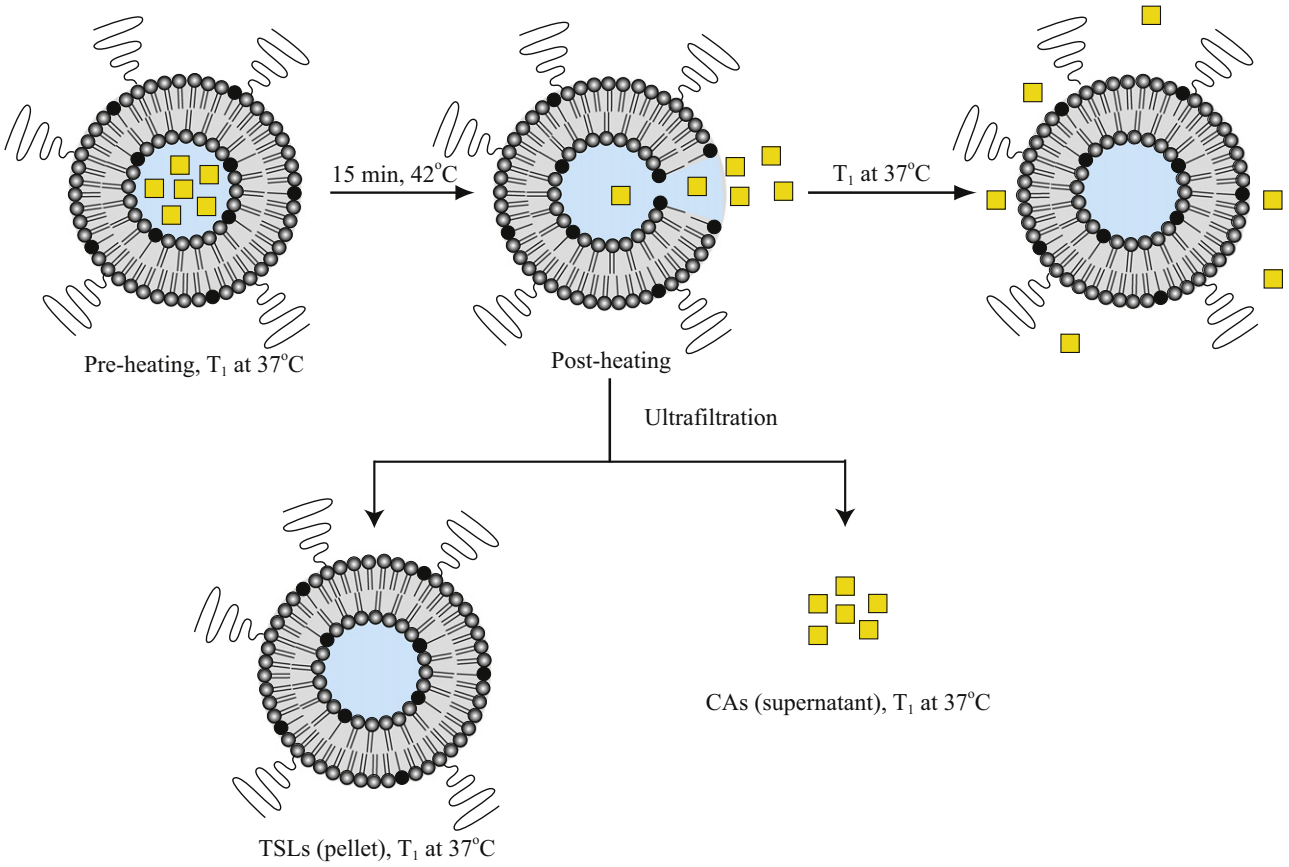

Fig. 2. Probing the release of encapsulated MRI CAs from the aqueous lumen of a TSL with T_1. Post heating, the released MRI CAs were physically separated from TSLs using 50 kDa Vivaspin ultrafiltration spin columns. Yellow squares represent MRI CAs ([Gd(HPDO3A)(H_2O)] or Mn^{2+}). This figure serves as a representation of the experimental steps taken and does not imply the absence of CA in the liposomal fraction (pellet) as well as potential interaction with phospholipid bilayer.

2.7. Stability of TSLs and release of Dox from TSLs

A fluorescence spectrometer (Perkin Elmer LS55) was used to study the release of Dox in a 300 mM sucrose/20 mM HEPES buffer, pH 7.5, at 37 and 41 °C over time. Signal intensity was estimated with λ_{ex} = 485 nm and λ_{em} = 590 nm. Subsequently, TSLs (2 μL) were added to the buffer (2 mL). Fluorescent intensity was measured every minute for one hour at 37 °C and every 15 s for 15 min at 41 °C. The percentage of Dox release was calculated according to Eq. (3),

$$\%\ \text{Dox release} = (I_t - I_0)/(I_{100} - I_0) \times 100\% \quad (3)$$

where I_t is the fluorescence intensity at a specific time, t, I_0 is the fluorescence intensity at t = 0, and I_{100} is the fluorescence intensity after addition of 5 μL 10% Trition X-100. Three different batches of liposomes were measured for each liposomal formulation.

Table 1
A summary of all measured samples with their respective CA, Dox and phospholipid concentrations.

Samples	[CA] mM	[Dox] μg/mL.	[Phospholipid] mM
TSL(Mn,Dox) pre heating	0.6	278	7.5
TSL(Mn,Dox) post heating	0.6	278	7.5
TSL + Mn + Dox	0.6	278	7.5
Mn + Dox	0.6	278	–
Mn^{2+}	0.6	–	–
TSL(Gd,Dox) pre heating	2.6	270	6.4
TSL(Gd,Dox) post heating	2.6	270	6.4
TSL + Mn + Dox	2.6	270	6.4
Gd + Dox	2.6	270	–
Gd(HPD03A)(H_20)	2.6	–	–

2.8. Release of intraliposomal contents during heating

The release of Dox was measured during heating from 25 to 50 °C (heating rate = 0.5 K/min) using a fluorescence spectrometer, whereas release of CAs was studied by measuring the T_1 during heating on a 300 MHz high-resolution NMR spectrometer (Bruker Avance, Ettlingen, Germany) from 25 to 50 °C (heating rate = 0.5 K/min) and followed by cooling down from 50 to 25 °C (cooling rate = 0.5 K/min). r_1 was calculated from the measured T_1 values using Eq. (1).

3. Results

3.1. Liposome preparation and characterization

TSLs containing Dox and Mn^{2+} [TSL(Mn,Dox)] or [Gd(HPDO3A)(H_2O)] [TSL(Gd,Dox)] were prepared containing DPPC, MPPC and DPPE-PEG_{2000} phospholipid in the lipid bilayer. DSC measurements showed that the T_m was 39.9 °C for both liposomal formulations. As evident from DLS, hydrodynamic radii of [TSL(Mn,Dox)] and [TSL(Gd,Dox)] were 58 and 57 nm, respectively. The average phospholipid, CA and Dox concentrations of TSLs are reported in Table 2. The morphology of liposomes and encapsulated Dox was studied by means of cryo-TEM. As shown in Fig. 3, before addition of Dox, TSL(Gd) were spherical, whereas TSL(Mn) displayed a faceted lipid bilayer morphology. The observed liposome morphologies were comparable to TSLs containing Mn^{2+} [29] and [Gd(HPDO3A)(H_2O)] [13] prepared by Chiu et al. and de Smet

Table 2
The average phospholipid, CA and Dox concentrations ± standard deviations of TSL(Mn, Dox) and TSL(Gd,Dox) (n = 3).

Liposomal formulations	[CA](mM)	[Phospholipid](mM)	[Dox](mM)
TSL(Mn,Dox)	0.54 ± 0.14	15.10 ± 1.37	0.62 ± 0.16
TSL(Gd,Dox)	4.53 ± 0.74	11.43 ± 1.10	0.95 ± 0.13

et al., respectively. Upon loading of Dox, stippled and diffuse Dox crystals were present in TSL(Mn,Dox) indicating Mn–Dox complex formation [28], while self-assembled fiber-like Dox crystals were evident in TSL(Gd,Dox) (Fig. 3) [13]. After heating, Dox crystals were absent in either of the TSLs, indicating complete release of Dox.

3.2. MR titration studies/binding studies

A titration study was performed to assess the interaction of MRI CAs with the phospholipid bilayer of TSLs. If MRI CAs were to interact with phospholipid bilayer, an increase in the rotational correlation time (τ_r) is expected leading to an increase in r_1 at 60 MHz. As shown in Fig. 4, with increasing phospholipid-to-MRI CA concentration ratio, an increase in r_1 was indeed observed for Mn^{2+} in contrast to [Gd(HPDO3A)(H_2O)] where change of r_1 was hardly observed. Taking the r_1 of Mn^{2+} as a fixed parameter with $r_{1,free} = 6.9\ mM^{-1}\ s^{-1}$, the data were fitted using the mathematical model describing the non-covalent binding of Mn^{2+} to the phospholipids [36,37]. The fit values found for TSL + Mn are $r_{1,\ bound} = 48.5\ mM^{-1}\ s^{-1}$, N = 0.04 and $K_a = 9.3 \times 10^4\ M^{-1}$, respectively.

3.3. Interaction of CAs with phospholipid bilayer after release

To further investigate whether the non-covalent interaction of the MRI CA with the phospholipid bilayer persists after release of encapsulated Mn^{2+} or [Gd(HPDO3A)(H_2O)] from TSLs, TSL(Mn), TSL(Mn,Dox), TSL(Gd) and TSL(Gd,Dox) were heated to 42 °C and cooled to 37 °C. Then, TSLs and the released intraliposomal contents were physically separated using Vivaspin ultrafiltration spin columns. T_1 data were measured at 37 °C and 60 MHz and r_1 values were calculated.

At 37 °C, r_1 of TSL(Mn) was 5.3 ± 0.9 $mM^{-1}\ s^{-1}$. After heating for 15 min at 42 °C, r_1 of TSL(Mn) at 37 °C increased to 34.7 ± 1.4 $mM^{-1}\ s^{-1}$ (Fig. 5). When TSL pellets and the supernatant containing the released intraliposomal contents were measured

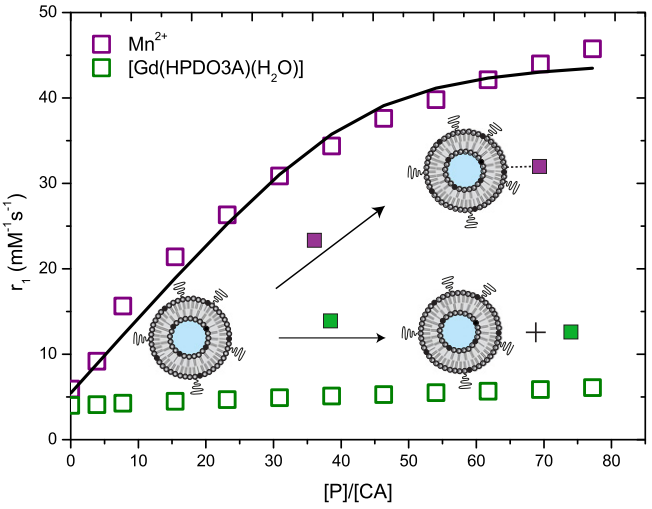

Fig. 4. Titration of TSLs to Mn^{2+} and [Gd(HPDO3A)(H_2O)] to investigate the interaction between phospholipid with MRI CAs on the r_1 at 60 MHz and 37 °C. The black line represents the fitted data.

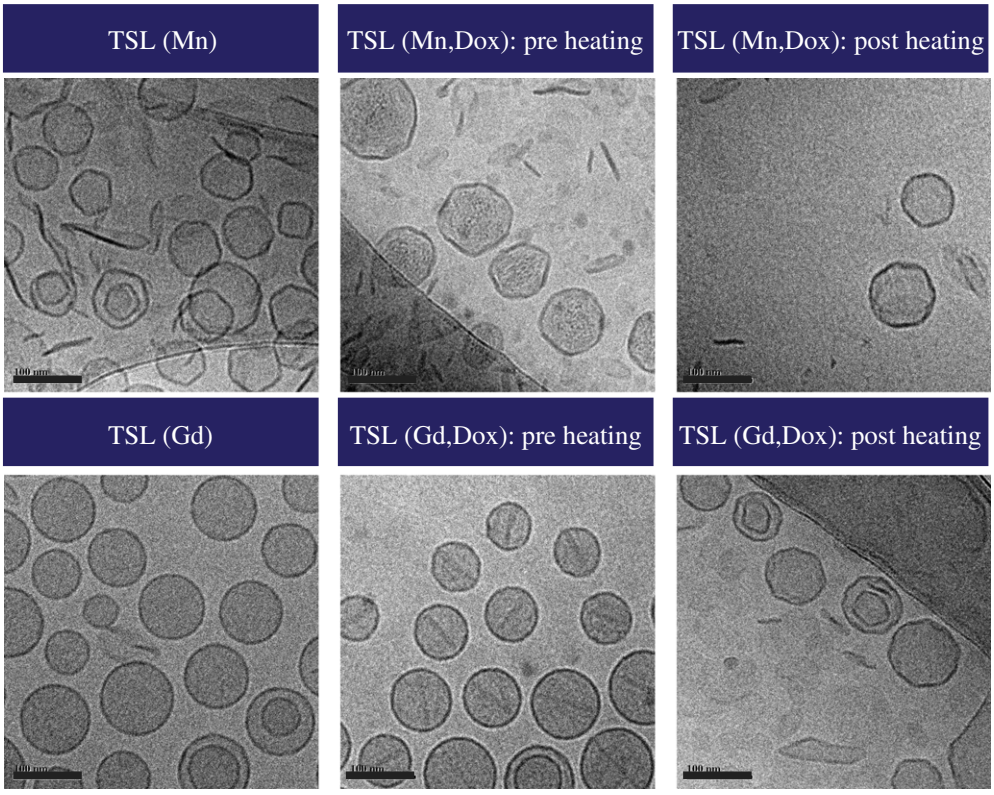

Fig. 3. CryoTEM images of TSLs loaded with Dox and MRI CAs. The scale bar represents 100 nm.

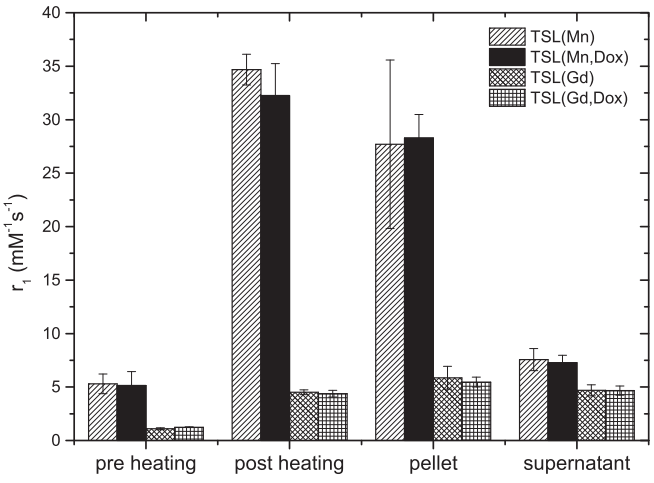

Fig. 5. An average change in $r_1 \pm$ SD of TSLs before and after heat treatment (n = 2). "pre heating" are samples without heat treatment; "post heating" are samples heated to 42 °C for 15 min and measured at 37 °C; "pellet" are samples subjected to centrifugation and containing TSLs; "supernatant" denotes samples subjected to centrifugation and containing released intraliposomal contents.

separately at 37 °C, the Mn^{2+} in the TSL pellets had an r_1 of 27.7 ± 7.9 $mM^{-1}\,s^{-1}$, while Mn^{2+} had a considerably lower r_1 of 7.6 ± 1.0 $mM^{-1}\,s^{-1}$ in the supernatant. Comparable results were obtained for TSL(Mn,Dox), with a r_1 of 5.1 ± 1.3 $mM^{-1}\,s^{-1}$ before heating and 32.2 ± 3.0 $mM^{-1}\,s^{-1}$ after heating. After separation, the r_1 of Mn^{2+} in TSL pellets and supernatant were 28.3 ± 2.2 $mM^{-1}\,s^{-1}$ and 7.3 ± 0.7 $mM^{-1}\,s^{-1}$.

For TSLs containing [Gd(HPDO3A)(H_2O)], TSL(Gd) displayed r_1 of 1.1 ± 0.1 $mM^{-1}\,s^{-1}$ at 37 °C and 4.5 ± 0.2 $mM^{-1}\,s^{-1}$ after heat treatment for 15 min (Fig. 5). In contrast to Mn^{2+} containing TSLs, the r_1 values of free [Gd(HPDO3A)(H_2O)] were 5.9 ± 1.1 $mM^{-1}\,s^{-1}$ in pellets and 4.7 ± 0.5 $mM^{-1}\,s^{-1}$ in supernatant. For the liposomal formulations encapsulating Dox, r_1 values of TSL(Gd,Dox) were 1.2 ± 0.03 $mM^{-1}\,s^{-1}$ before and 4.4 ± 0.3 $mM^{-1}\,s^{-1}$ after heating. After separation, r_1 of [Gd(HPDO3A)(H_2O)] in TSL pellets was 5.5 ± 0.5 $mM^{-1}\,s^{-1}$ and 4.7 ± 0.4 $mM^{-1}\,s^{-1}$ in supernatant.

3.4. ^1H nuclear magnetic relaxation dispersion (NMRD)

^1H NMRD profiles for all samples listed in Table 1 were measured at 35 °C to prevent premature release of CAs from interior of the liposomes. Before heating, the apparent r_1 of the TSL(Mn,Dox) was lower than that of Mn + Dox and Mn^{2+} solutions at magnetic fields ranging from 0.02 to 300 MHz (Fig. 6a). This apparent reduction of r_1 with respect to free Mn^{2+} is due to the limited transmembrane water exchange across the phospholipid bilayer [38]. NMRD for Mn + Dox was similar to free Mn^{2+} suggesting no observable influence of Dox on r_1 of Mn^{2+} at the measured concentration. The Mn + Dox profile showed the classic behavior of aqueous Mn^{2+} ions where a first dispersion was observed around 0.1 MHz due to scalar interaction and a second dispersion was around 7 MHz due to dipolar interaction. After heating of the TSL, the release of Mn + Dox from the interior of the liposomes caused an increase in the r_1 (Fig. 6a). The increase in r_1 is more prominent at magnetic fields ranging from 3 to 60 MHz (Fig. 6a). It is important to note that at magnetic fields higher than 0.3 MHz, the r_1 of TSL(Mn,Dox) after heating is higher than the Mn + Dox solution, suggesting binding of Mn^{2+} to the phospholipid bilayer. Interestingly, the ^1H NMRD profiles of TSL + Mn + Dox were higher as compared to TSL(Mn, Dox) post heating with the exception of magnetic field 0.3 MHz

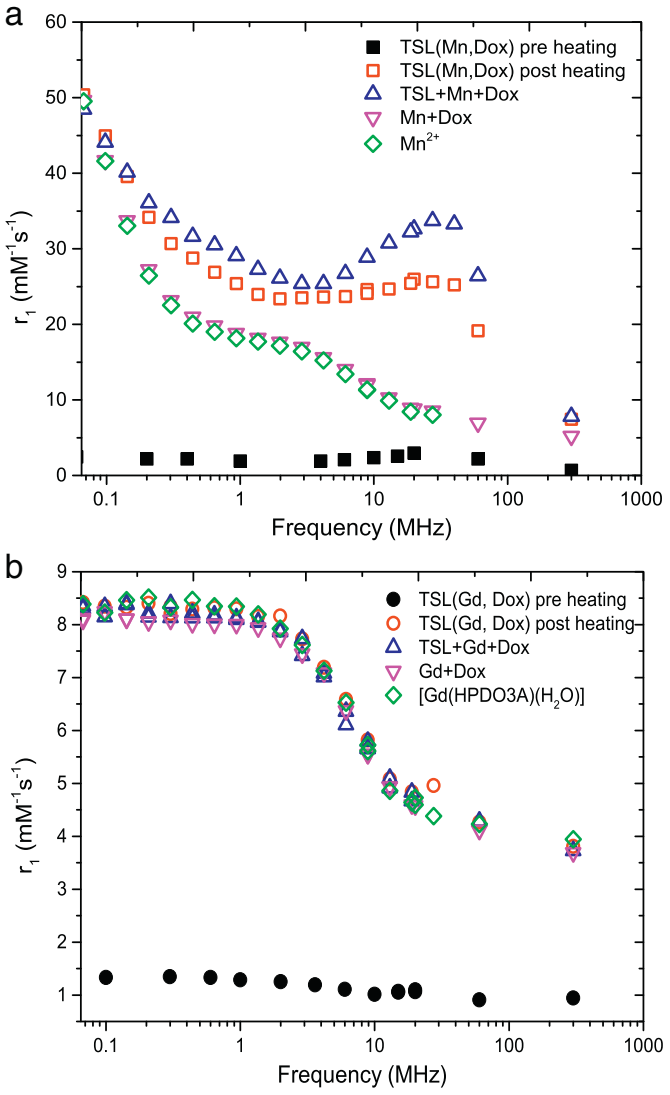

Fig. 6. (a) ^1H NMRD profiles of TSL(Mn,Dox) pre and post heating, TSL + Mn + Dox, Mn + Dox and Mn^{2+} solutions; (b) ^1H NMRD profiles of TSL(Gd,Dox) pre and post heating, TSL + Gd + Dox, Gd + Dox and [Gd(HPDO3A)(H_2O)].

and below. This can be explained by an increased number of Mn^{2+} bound to the exterior phospholipids in the TSL + Mn + Dox when Mn^{2+} was added to a TSL sample. On the other hand, after heating and cooling of TSL(Mn,Dox), Mn^{2+} ions could be interacting with the inner layer of the phospholipid bilayer, leading to re-encapsulation of Mn^{2+} in the interior of the liposomes and thus, resulting in a lower r_1 as compared to TSL + Mn + Dox.

At magnetic field strengths of 0.02 to 300 MHz, TSL(Gd,Dox) has a r_1 lower than Gd + Dox and [Gd(HPDO3A)(H_2O)] solution before heat treatment (Fig. 6b) due to limited transmembrane water exchange. In line with earlier measurements [18], r_1 values were higher and similar to those of Gd + Dox solution following heat treatment of TSL(Gd,Dox). External addition of Gd + Dox to empty TSLs also did not affect the r_1 (Fig. 6b). All these data show that the contribution of non-covalent interactions between the [Gd(HPDO3A)(H_2O)] and the phospholipid bilayer is limited. Furthermore, complete release of [Gd(HPDO3A)(H_2O)] from the lumen of the TSLs occurred. These observations were consistent with results on Fig. 5. The NMRD profiles of Gd-Dox and [Gd(HPDO3A)(H_2O)] were representative of low molecular weight Gd-chelate CAs.

3.5. Stability of TSLs and release of Dox

TSLs were designed to stably encapsulate intraliposomal contents at 37 °C and exhibit rapid release of intraliposomal contents at hyperthermic conditions (>40 °C). The stability and release of Dox were assessed using fluorimetry at 37 and 41 °C. Following 2 min of heating at 41 °C, TSL(Mn,Dox) and TSL(Gd,Dox) exhibited rapid release of Dox up to 86 ± 3% and 98 ± 3%, respectively (Fig. 7). At 37 °C, TSL(Mn,Dox) showed Dox released up to 61 ± 13% over a period of one hour, whereas TSL(Gd,Dox) showed gradual release of Dox up to 12 ± 8% (Fig. 7a).

3.6. Release of intraliposomal contents during heating

The release profiles of the two MRI CAs and Dox from TSLs were investigated where the release of Dox was followed using fluorescence spectroscopy and the release of MRI CAs was followed using a 300 MHz NMR spectrometer. For the latter, the apparent r_1 was calculated from the measured R_1 ($1/T_1$) and the CA concentrations.

As the temperature was raised from 25 to 50 °C, Dox was gradually released from TSL(Mn,Dox), with a sharp release starting at 38.3 °C (Fig. 8a). Concurrently, the release profile of Mn^{2+}, plotted as r_1, clearly parallels the release profile of Dox. Upon cooling, r_1 remained high and increased with decreasing temperatures. For temperatures below the T_m of the TSLs, this increase is smaller compared to the temperature range above T_m. The trend of the observed Mn^{2+} release profile matches the Mn^{2+} release profile from TSL (DPPC/MSPC/DSPE-PEG_{2000}) measured at 85 MHz [9].

TSL(Gd,Dox) remained stable at low temperature and exhibited a rapid release of Dox at 37.3 °C. The the gradual increase in r_1 from 25 to 38 °C was due to increased transmembrane water exchange, an effect of temperature increase. From 38 °C, the irreversible release of [Gd(HPDO3A)(H_2O)] clearly coincided with the release of Dox. These results verify that there were simultaneous releases of Dox and [Gd(HPDO3A)(H_2O)], which are consistent with results reported by de Smet et al. using similar liposomal formulation [13] and Negussie et al. using different TSL formulation (DPPC/MSPC/DSPE-PEG_{2000}) [18].

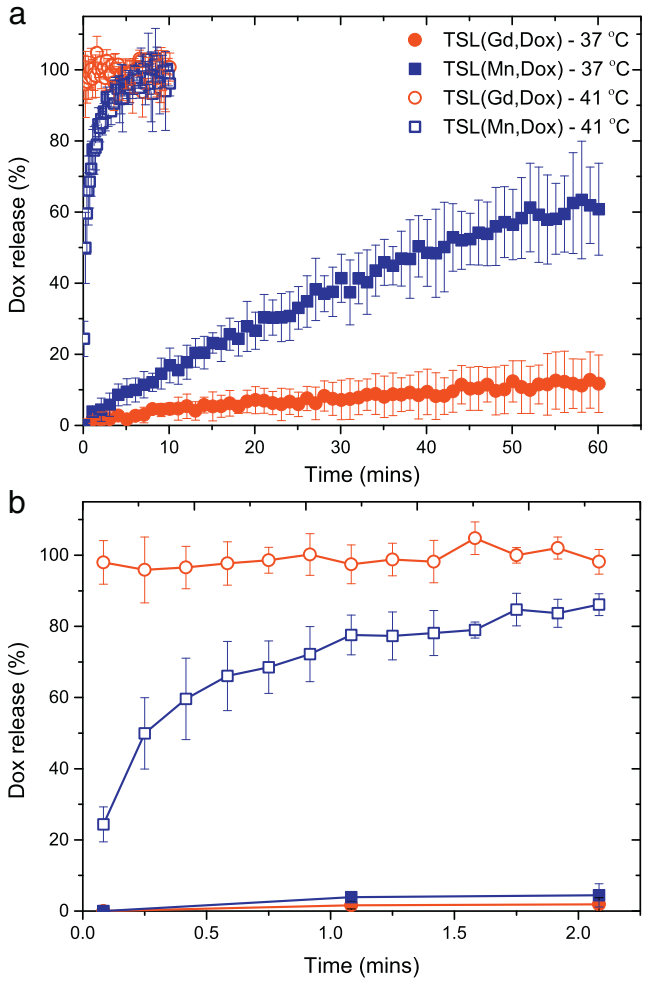

Fig. 7. (a) Stability and release of Dox in HEPES buffered saline (HBS), pH 7.5, at 37 and 41 °C, respectively (n = 3). Dox release was plotted as average of percentages ± SD. (b) Release kinetics of Dox within the first 2 min at 37 and 41 °C.

4. Discussions

TSLs co-encapsulating MRI CAs and drug in their aqueous lumen offer the prospect of visualization and quantification of drug release using MRI. Here, the effects of co-encapsulating Mn^{2+} or [Gd(HPDO3A)(H_2O)] with Dox and the interaction of Mn^{2+} and [Gd(HPDO3A)(H_2O)] with the phospholipid bilayer were investigated and compared through cryo TEM images, stability and release studies, MR titration studies and ^{1}H NMRD profiles measurements.

As expected, at temperatures lower than T_m, the limited water exchange across the liposomal membrane results in low r_1 of TSL(Mn, Dox) and TSL(Gd,Dox) samples. After heating above the T_m, the r_1 increased for both types of liposomes, but a major difference is observed between Mn^{2+}- or [Gd(HPDO3A)(H_2O)]-loaded liposomes. For Mn^{2+}-loaded liposomes, the NMRD profiles show a hump in the high field region (10 to 100 MHz) typical of an interaction of Mn^{2+} ions with macromolecular systems whereas, for [Gd(HPDO3A)(H_2O)]-loaded liposomes, identical r_1 values were measured on the whole magnetic field range for [Gd(HPDO3A)(H_2O)]-loaded TSLs, TSLs with external [Gd(HPDO3A)(H_2O)], [Gd(HPDO3A)(H_2O)] in presence of Dox and [Gd(HPDO3A)(H_2O)]. These data confirm the release of Mn^{2+} ions and [Gd(HPDO3A)(H_2O)] as well as a non-covalent interaction of Mn^{2+} with phospholipids, which is clearly not observed for [Gd(HPDO3A)(H_2O)].

The MR titration and binding studies were performed with the aim to assess and quantify the interaction of CA with the negatively charged phospholipid head groups. It is evident that Mn^{2+}, titrated with empty TSL or after hyperthermia mediated release from the interior of the liposomes, interacts with the negatively charged phospholipid bilayer, which is in line with results from Caride et al. [16]. This interaction slowed down the molecular tumbling rate of Mn^{2+} and thus, resulted in r_1 values higher than those of free Mn^{2+} [10,39]. This observation is supported by Koenig et al., who showed that when unilamellar phosphatidylserine vesicles were added to Mn^{2+}, the binding of Mn^{2+} to the vesicles caused an increase in r_1 up to approximately 42 mM^{-1} s^{-1} (20 MHz) [38]. The increase was most significant at low magnetic fields and gradually decreased at higher magnetic fields [38]. The derived K_a indicated non-covalent interactions between Mn^{2+} and the phospholipid bilayer. This explained the lower r_1 of the pellet fraction of TSL(Mn) and TSL(Mn,Dox) as compared to their respective TSL post heating (Fig. 5). The lower r_1 measured in the pellet fractions of TSL(Mn) and TSL(Mn,Dox) might be due a mixture of TSL-bound Mn^{2+} and free Mn^{2+} in the solution. For in vivo applications, the observed interaction between Mn^{2+} and phospholipid bilayer is valuable for several reasons. Cellular toxicity has always been a setback for clinical applications of Mn^{2+} [31–33]. To date, only Mn-DPDP (Teslascan®) has been approved for clinical applications at a dose of 5 μmol/kg [40] or 10 μmol/kg [41]. For our formulation, a delivery of 0.5–1.3 mg/kg Dox (=20–50 mg/m^2) [42–44], which is a typical dose applied in clinical settings for Doxil® (a clinically approved pegylated non temperature-sensitive liposomal formulation of Dox), would result in a Mn^{2+} dose of 0.8–2.0 μmol/kg. This range of Mn^{2+} doses is lower than Teslascan®, making TSL(Mn,Dox) formulation an attractive candidate for clinical

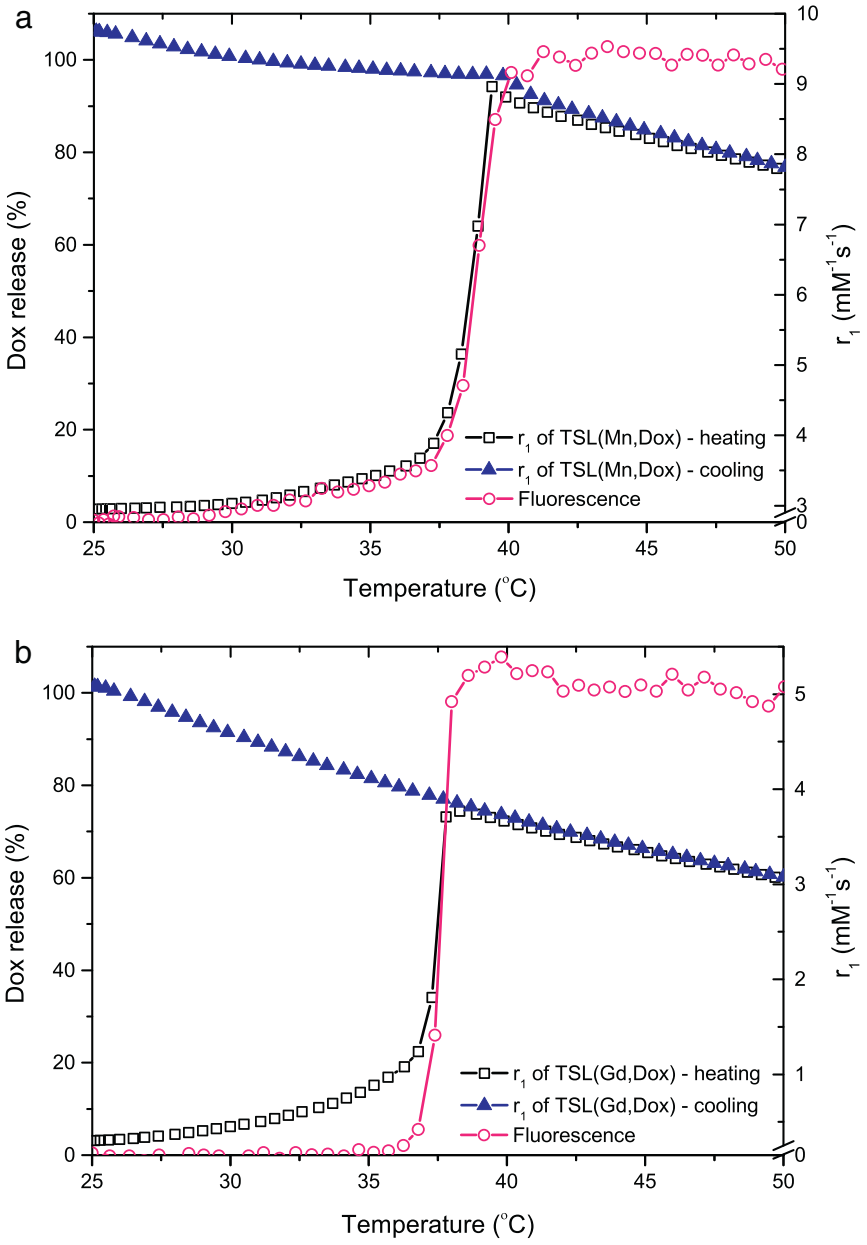

Fig. 8. (a) The release of Dox and Mn^{2+} from TSL(Mn,Dox) during heating from 25 to 50 °C (0.5 K/min), measured as a function of change in fluorescence intensity and r_1 at 300 MHz magnetic field, respectively. (b) The release of Dox and [Gd(HPDO3A)(H_2O)] from TSL(Gd,Dox).

applications. The non-covalent interaction between Mn^{2+} and the negatively charged phospholipids of the TSL is likely beneficial for applications in MR image-guided Dox delivery in tumors with a high vascular permeability. Interaction of Mn^{2+} with phospholipids in tumor environments will result in slower downstream wash out of Mn^{2+} as compared to [Gd(HPDO3A)(H_2O)] (an extracellular CA), hence enables better correlation of MRI signals with local drug distributions in tumors.

Our study suggests that Mn^{2+} has an effect on the stability (drug retention) of TSLs as compared to [Gd(HPDO3A)(H_2O)] at 37 °C. Interaction of Mn^{2+} with phospholipid bilayer resulted in higher leakage of Dox from the interior of TSLs as compared to the leakage from a comparable formulation, but containing [Gd(HPDO3A)(H_2O)] instead of Mn^{2+}. Another possible explanation for the TSL(Mn,Dox) instability might be the nature of the Dox precipitation within the liposomes (Fig. 3). Abraham et al. have shown that liposomes encapsulating Dox contained fibrous-bundle aggregates of Dox precipitation [28]. However, cryo-TEM images of liposomes containing both Mn^{2+} and Dox (Fig. 3) did not show similar Dox precipitation due to complexation of Mn^{2+} with Dox. The absence of self-assembled fiber-like structure as seen in TSL(Gd,Dox) [13], coupled with the diffusion of Mn–Dox complexes across the phospholipid bilayer might be the contributing reasons to the leakage of Dox at 37 °C. In addition, studies have shown that the presence of transmembrane pH gradient plays a critical role in the retention of Dox in liposomes [45]. However, the addition of Mn^{2+} was reported to cause a loss of transmembrane pH gradient [30], which may contribute to a higher leakage of Dox from TSL(Mn,Dox) at body temperature. For future applications using TSL(Mn), phospholipids with higher T_m could be used to improve the stability of TSL(Mn), though any compromise on the rapid release kinetic at hyperthermic temperature needs to be avoided. Alternatively, Dox could be loaded via complexation with Mn^{2+} in the presence of triethanolamine (TEA) at neutral pH. In a comprehensive study, Kheirolomoom et al. showed that Dox loading via a copper/TEA gradient improved the drug retention capability in the interior of the liposomes at pH 7.4–8.5

and complexation between copper and Dox [46,47]. However, this loading method needs to be further assessed for incorporation of Mn^{2+} and Dox within the interior of TSLs.

Consistent with previous results, encapsulation of [Gd(HPDO3A)(H_2O)] did not affect the stability of TSL(Gd, Dox) [13,18]. Also, results did not show interaction of [Gd(HPDO3A)(H_2O)] with the negatively charged phospholipid bilayer. One disadvantage of the absence of [Gd(HPDO3A)(H_2O)] and phospholipid interaction is that [Gd(HPDO3A)(H_2O)] as an extracellular CA can be rapidly washed out from the tumor tissues. However, [Gd(HPDO3A)(H_2O)] is a clinically approved MRI CA [48] and Negussie et al. showed that 150 μmol/kg of [Gd(HPDO3A)(H_2O)] is required for MRI [18]. This concentration is well below its LD_{50} (mice = 12,000 μmol/kg) [49] and comparable to the diagnostic dose of 100–300 μmol/kg [50]. From this perspective, clinical translation of TSL(Gd,Dox) is more achievable as compared to TSL(Mn,Dox).

With the introduction of MRI guided High Intensity Focused Ultrasound (MR-HIFU) to induce hyperthermia non-invasively, paramagnetic TSLs become a more attractive and desirable option to transport drugs to diseased tissues. Preclinical studies thereafter also consistently show that MR-HIFU induced hyperthermia was able to increase drug concentration at tumor tissues compared to non-HIFU treated tumors [2,51]. The recent development and application of TSLs in combination with MR-HIFU for drug delivery has been reviewed in detail [52–54]. Given the demonstrated ability of paramagnetic TSLs for image guided drug delivery, the influence of Mn^{2+} and [Gd(HPDO3A)(H_2O)] on TSL stability and MRI signal enhancement (ΔR_1) should be well understood to ensure accurate interpretation of drug dosage delivery in vivo.

5. Conclusions

The non-covalent interactions of encapsulated MRI CAs with the phospholipid bilayer of the TSLs can be a double-edged sword. Though the interaction of Mn^{2+} with the phospholipid head groups reduced the drug retention capability of the TSLs as compared to [Gd(HPDO3A)(H_2O)], the increase in r_1 due to Mn–phospholipid interaction can be exploited to reduce Mn^{2+} concentration in vivo. In addition, the interaction of Mn^{2+} with the phospholipids of the targeted tissue can lead to a prolonged retention of Mn^{2+} in situ, which makes drug quantification more independent of the exact perfusion of the tumor. Equipped with thorough understanding of CA-phospholipid interactions, TSLs can be designed to incorporate different phospholipids in combination with Mn^{2+} or [Gd(HPDO3A)(H_2O)] for MR guided drug delivery.

Acknowledgements

This research was performed within the framework of CTMM, the Center for Translational Molecular Medicine (www.ctmm.nl), project HIFU-CHEM (grant 03O-301) and COST Action TD1004.

References

[1] M. Yatvin, J. Weinstein, W. Dennis, R. Blumenthal, Design of liposomes for enhanced local release of drugs by hyperthermia, Science 202 (1978) 1290–1293.
[2] M. de Smet, E. Heijman, S. Langereis, N.M. Hijnen, H. Grüll, Magnetic resonance imaging of high intensity focused ultrasound mediated drug delivery from temperature-sensitive liposomes: an *in vivo* proof-of-concept study, J. Control. Release 150 (2011) 102–110.
[3] D. Needham, G. Anyarambhatla, G. Kong, M.W. Dewhirst, A new temperature-sensitive liposome for use with mild hyperthermia: characterization and testing in a human tumor xenograft model, Cancer Res. 60 (2000) 1197–1201.
[4] P.S. Yarmolenko, Y. Zhao, C. Landon, I. Spasojevic, F. Yuan, D. Needham, B.L. Viglianti, M.W. Dewhirst, Comparative effects of thermosensitive doxorubicin-containing liposomes and hyperthermia in human and murine tumours, Int. J. Hyperth. 26 (2010) 485–498.
[5] G.R. Anyarambhatla, D. Needham, Enhancement of the phase transition permeability of DPPC liposomes by incorporation of MPPC: a new temperature-sensitive liposome for use with mild hyperthermia, J. Liposome Res. 9 (1999) 491–506.
[6] J.K. Mills, D. Needham, Lysolipid incorporation in dipalmitoylphosphatidylcholine bilayer membranes enhances the ion permeability and drug release rates at the membrane phase transition, Biochim. Biophys. Acta Biomembr. 1716 (2005) 77–96.
[7] C.D. Landon, J.Y. Park, D. Needham, M.W. Dewhirst, Nanoscale drug delivery and hyperthermia: the materials design and preclinical and clinical testing of low temperature-sensitive liposomes used in combination with mild hyperthermia in the treatment of local cancer, Open Nanomedicine J. 3 (2011) 38–64.
[8] A.M. Ponce, B.L. Viglianti, D. Yu, P.S. Yarmolenko, C.R. Michelich, J. Woo, M.B. Bally, M.W. Dewhirst, Magnetic resonance imaging of temperature-sensitive liposome release: drug dose painting and antitumor effects, J. Natl. Cancer Inst. 99 (2007) 53–63.
[9] B.L. Viglianti, S.A. Abraham, C.R. Michelich, P.S. Yarmolenko, J.R. MacFall, M.B. Bally, M.W. Dewhirst, *In vivo* monitoring of tissue pharmacokinetics of liposome/drug using MRI: illustration of targeted delivery, Magn. Reson. Med. 51 (2004) 1153–1162.
[10] B.L. Viglianti, A.M. Ponce, C.R. Michelich, D. Yu, S.A. Abraham, L. Sanders, P.S. Yarmolenko, T. Schroeder, J.R. MacFall, D.P. Barboriak, O.M. Colvin, M.B. Bally, M. W. Dewhirst, Chemodosimetry of *in vivo* tumor liposomal drug concentration using MRI, Magn. Reson. Med. 56 (2006) 1011–1018.
[11] H.M. Reinl, M. Hossann, L.H. Lindner, M. Reise, in: O. Dössel, W.C. Schlege (Eds.), Thermosensitive Mn^{2+}-liposomes for MR-guided hyperthermia — Solvent-dependent Mn^{2+} Release World Congress on Medical Physics and Biomedical Engineering, September 7–12, 2009, vol. 25/13, Springer Berlin Heidelberg, Munich, Germany, 2010, pp. 21–22.
[12] M. de Smet, N.M. Hijnen, S. Langereis, A. Elevelt, E. Heijman, L. Dubois, P. Lambin, H. Grüll, Magnetic resonance guided high-intensity focused ultrasound mediated hyperthermia improves the intratumoral distribution of temperature-sensitive liposomal Doxorubicin, Invest. Radiol. 48 (2013) 395–405.
[13] M. de Smet, S. Langereis, S.v. den Bosch, H. Grüll, Temperature-sensitive liposomes for doxorubicin delivery under MRI guidance, J. Control. Release 143 (2010) 120–127.
[14] M. de Smet, S. Langereis, S. van den Bosch, K. Bitter, N. Hijnen, E. Heijman, H. Grüll, SPECT/CT imaging of temperature-sensitive liposomes for MR-image guided drug delivery with high intensity focused ultrasound, J. Control. Release 169 (2013) 82–90.
[15] G. Bacić, M.R. Niesman, H.F. Bennett, R.L. Magin, H.M. Swartz, Modulation of Water Proton Relaxation Rates by Liposomes Containing Paramagnetic Materials, 1988.
[16] V.J. Caride, H.D. Sostman, R.J. Winchell, J.C. Gore, Relaxation enhancement using liposomes carrying paramagnetic species, Magn. Reson. Imaging 2 (1984) 107–112.
[17] L. Frich, A. Bjørnerud, S. Fossheim, T. Tillung, I. Gladhaug, Experimental application of thermosensitive paramagnetic liposomes for monitoring magnetic resonance imaging guided thermal ablation, Magn. Reson. Med. 52 (2004) 1302–1309.
[18] A.H. Negussie, P.S. Yarmolenko, A. Partanen, A. Ranjan, G. Jacobs, D. Woods, H. Bryant, D. Thomasson, M.W. Dewhirst, B.J. Wood, M.R. Dreher, Formulation and characterisation of magnetic resonance imageable thermally sensitive liposomes for use with magnetic resonance-guided high intensity focused ultrasound, Int. J. Hyperth. 27 (2011) 140–155.
[19] M. Peller, A. Schwerdt, M. Hossann, H.M. Reinl, T. Wang, S. Sourbron, M. Ogris, L.H. Lindner, MR characterization of mild hyperthermia-induced gadodiamide release from thermosensitive liposomes in solid tumors, Invest. Radiol. 43 (2008) 877–892.
[20] T. Tagami, W.D. Foltz, M.J. Ernsting, C.M. Lee, I.F. Tannock, J.P. May, S.-D. Li, MRI monitoring of intratumoral drug delivery and prediction of the therapeutic effect with a multifunctional thermosensitive liposome, Biomaterials 32 (2011) 6570–6578.
[21] S.L. Fossheim, K.A. Il'yasov, J. Hennig, A. Bjørnerud, Thermosensitive paramagnetic liposomes for temperature control during MR imaging-guided hyperthermia: in vitro feasibility studies, Acad. Radiol. 7 (2000) 1107–1115.
[22] K.A. Il'yasov, S.L. Fossheim, U.N. Wiggen, A. Rogstad, J. Hennig, A. Bjørnerud, Paramagnetic liposomes as thermosensitive probes for MRI-guided thermal treatment: in vitro feasibility studies, Appl. Magn. Reson. 33 (2008) 469–480.
[23] N. McDannold, S.L. Fossheim, H. Rasmussen, H. Martin, N. Vykhodtseva, K. Hynynen, Heat-activated liposomal MR contrast agent: initial *in vivo* results in rabbit liver and kidney1, Radiology 230 (2004) 743–752.
[24] C. Bos, M. Lepetit-Coiffé, B. Quesson, C.T.W. Moonen, Simultaneous monitoring of temperature and T1: methods and preliminary results of application to drug delivery using thermosensitive liposomes, Magn. Reson. Med. 54 (2005) 1020–1024.
[25] T. Wang, M. Hossann, H.M. Reinl, M. Peller, H. Eibl, M. Reiser, R.D. Issels, L.H. Lindner, In vitro characterization of phosphatidylglyceroglycerol-based thermosensitive liposomes with encapsulated 1H MR T1-shortening gadodiamide, Contrast Media Mol. Imaging 3 (2008) 19–26.
[26] S.L. Fossheim, A.K. Fahlvik, J. Klaveness, R.N. Muller, Paramagnetic liposomes as MRI contrast agents: influence of liposomal physicochemical properties on the in vitro relaxivity, Magn. Reson. Imaging 17 (1999) 83–89.
[27] S.H. Koenig, Q.F. Ahkong, R.D. Brown, M. Lafleur, M. Spiller, E. Unger, C. Tilcock, Permeability of liposomal membranes to water: results from the magnetic field dependence of T1 of solvent protons in suspensions of vesicles with entrapped paramagnetic ions, Magn. Reson. Med. 23 (1992) 275–286.
[28] S.A. Abraham, K. Edwards, G. Karlsson, S. MacIntosh, L.D. Mayer, C. McKenzie, M.B. Bally, Formation of transition metal–doxorubicin complexes inside liposomes, Biochim. Biophys. Acta 1565 (2002) 41–54.
[29] G.N. Chiu, S.A. Abraham, L.M. Ickenstein, R. Ng, G. Karlsson, K. Edwards, E.K. Wasan, M.B. Bally, Encapsulation of doxorubicin into thermosensitive liposomes via complexation with the transition metal manganese, J. Control. Release 104 (2005) 271–288.
[30] S.A. Abraham, D.N. Waterhouse, L.D. Mayer, P.R. Cullis, T.D. Madden, M.B. Bally, The liposomal formulation of doxorubicin, Methods Enzymol. 391 (2005) 71–97.

[31] A.P. Koretsky, A.C. Silva, Manganese-enhanced magnetic resonance imaging (MEMRI), NMR Biomed. 17 (2004) 527–531.
[32] A.C. Silva, J.H. Lee, I. Aoki, A.P. Koretsky, Manganese-enhanced magnetic resonance imaging (MEMRI): methodological and practical considerations, NMR Biomed. 17 (2004) 532–543.
[33] G. Wolf, L. Baum, Cardiovascular toxicity and tissue proton T1 response to manganese injection in the dog and rabbit, Am. J. Roentgenol. 141 (1983) 193–197.
[34] M.N. Eakins, S.M. Eaton, R.A. Fisco, R.J. Hunt, C.E. Ita, T. Katona, L.M. Owies, E. Schramm, J.W. Sulner, C.W. Thompson, G.W. White, S. Murthy Yerramilli, Physicochemical properties, pharmacokinetics, and biodistribution of gadoteridol injection in rats and dogs, Acad. Radiol. 2 (1995) 584–591.
[35] G. Rouser, S. Fleischer, A. Yamamoto, Two dimensional thin layer chromatographic separation of polar lipids and determination of phospholipids by phosphorus analysis of spots, Lipids 5 (1970) 494–496.
[36] S. Langereis, H.-A.T. Kooistra, M.H.P. van Genderen, E.W. Meijer, Probing the interaction of the biotin–avidin complex with the relaxivity of biotinylated Gd-DTPA, Org. Biomol. Chem. 2 (2004) 1271–1273.
[37] I. Tinoco, K. Sauer, J.C. Wang, Physical Chemistry: Principles and Applications in Biological Sciences, 3rd ed., 1995. Chapter 11.
[38] S.H. Koenig, R.D. Brown 3rd, R. Kurland, S. Ohki, Relaxivity and binding of Mn2+ ions in solutions of phosphatidylserine vesicles, Magn. Reson. Med. 7 (1988) 133–142.
[39] É. Tóth, L. Helm, A. Merbach, in: W. Krause (Ed.), Relaxivity of MRI Contrast Agents Contrast Agents I, vol. 221, Springer Berlin/ Heidelberg, 2002, pp. 61–101.
[40] M.P. Federle, J.L. Chezmar, D.L. Rubin, J.C. Weinreb, P.C. Freeny, R.C. Semelka, J.J. Brown, J.A. Borrello, J.K.T. Lee, R. Mattrey, A.H. Dachman, S. Saini, B. Harmon, M. Fenstermacher, R.E. Pelsang, S.E. Harms, D.G. Mitchell, H.H. Halford Iii, M.W. Anderson, C.D. Johnson, I.R. Francis, J.G. Bova, P.J. Kenney, D.L. Klippenstein, G.S. Foster, D.A. Turner, A.E. Stillman, R.C. Nelson, S.W. Young, R.H. Patt, M. Rifkin, S.E. Seltzer, S.B. Gay, R.O. Robison, P.F. Sherwin, R. Ballerini, Safety and efficacy of mangafodipir trisodium (MnDPDP) injection for hepatic MRI in adults: results of the U.S. Multicenter Phase III Clinical Trials (Safety), J. Magn. Reson. Imaging 12 (2000) 186–197.
[41] W. Schima, R. Függer, E. Schober, C. Oettl, P. Wamser, F. Grabenwöger, J.M. Ryan, G. Novacek, Diagnosis and staging of pancreatic cancer: comparison of mangafodipir trisodium—enhanced MR imaging and contrast-enhanced helical hydro-CT, Am. J. Roentgenol. 179 (2002) 717–724.
[42] Y. Barenholz, Doxil® — the first FDA-approved nano-drug: lessons learned, J. Control. Release 160 (2012) 117–134.
[43] R.M. Rifkin, S.A. Gregory, A. Mohrbacher, M.A. Hussein, Pegylated liposomal doxorubicin, vincristine, and dexamethasone provide significant reduction in toxicity compared with doxorubicin, vincristine, and dexamethasone in patients with newly diagnosed multiple myeloma, Cancer 106 (2006) 848–858.
[44] S. Stewart, H. Jablonowski, F.D. Goebel, K. Arasteh, M. Spittle, A. Rios, D. Aboulafia, J. Galleshaw, B.J. Dezube, Randomized comparative trial of pegylated liposomal doxorubicin versus bleomycin and vincristine in the treatment of AIDS-related Kaposi's sarcoma. International Pegylated Liposomal Doxorubicin Study Group, J. Clin. Oncol. 16 (1998) 683–691.
[45] L.D. Mayer, L.C.L. Tai, M.B. Bally, G.N. Mitilenes, R.S. Ginsberg, P.R. Cullis, Characterization of liposomal systems containing doxorubicin entrapped in response to pH gradients, Biochim. Biophys. Acta Biomembr. 1025 (1990) 143–151.
[46] A. Kheirolomoom, C.-Y. Lai, S.M. Tam, L.M. Mahakian, E.S. Ingham, K.D. Watson, K.W. Ferrara, Complete regression of local cancer using temperature-sensitive liposomes combined with ultrasound-mediated hyperthermia, J. Control. Release 172 (2013) 266–273.
[47] A. Kheirolomoom, L.M. Mahakian, C.-Y. Lai, H.A. Lindfors, J.W. Seo, E.E. Paoli, K.D. Watson, E.M. Haynam, E.S. Ingham, L. Xing, R.H. Cheng, A.D. Borowsky, R.D. Cardiff, K.W. Ferrara, Copper–doxorubicin as a nanoparticle cargo retains efficacy with minimal toxicity, Mol. Pharm. 7 (2010) 1948–1958.
[48] M.F. Tweedle, The ProHance story: the making of a novel MRI contrast agent, Eur. Radiol. 7 (1997) S225–S230.
[49] A.N. Oksendal, P.-A. Hals, Biodistribution and toxicity of MR imaging contrast media, J. Magn. Reson. Imaging 3 (1993) 157–165.
[50] N.a.E., N. Karabukut, Contrast agents used in MR imaging of the liver, Diagn. Interv. Radiol. 12 (2006) 22–30.
[51] A. Ranjan, G.C. Jacobs, D.L. Woods, A.H. Negussie, A. Partanen, P.S. Yarmolenko, C.E. Gacchina, K.V. Sharma, V. Frenkel, B.J. Wood, M.R. Dreher, Image-guided drug delivery with magnetic resonance guided high intensity focused ultrasound and temperature sensitive liposomes in a rabbit Vx2 tumor model, J. Control. Release 158 (2012) 487–494.
[52] H. Grüll, S. Langereis, Hyperthermia-triggered drug delivery from temperature-sensitive liposomes using MRI-guided high intensity focused ultrasound, J. Control. Release 161 (2012) 317–327.
[53] N. Hijnen, S. Langereis, H. Grüll, Magnetic resonance guided high-intensity focused ultrasound for image-guided temperature-induced drug delivery, Adv. Drug Deliv. Rev. 72 (2014) 65–81.
[54] S. Langereis, T. Geelen, H. Grüll, G.J. Strijkers, K. Nicolay, Paramagnetic liposomes for molecular MRI and MRI-guided drug delivery, NMR Biomed. 26 (2013) 728–744.